DESIGN AND NUMERICAL ANALYSIS OF A ROOM-SIZED VOLUMETRIC RESONATOR FOR UBIQUITOUS WIRELESS POWER TRANSFER

***Charoskhon Sevinchova*[1]**

***Pavel Belov*[1]**

[1] *Department of Modern Physics, School of Engineering, New Uzbekistan University, Tashkent, Uzbekistan*

Abstract. *Conventional inductive wireless charging confines power transfer to a thin layer above a planar coil, requiring precise alignment and leaving pronounced dead zones in three-dimensional space. This paper reports the design and full-wave numerical analysis of a room-sized volumetric resonator intended for ubiquitous wireless power transfer (WPT) in a smart-home environment. A resonant structure occupying a 3.35 × 3.35 × 2.5 m volume was modelled in CST Studio Suite together with a compact receiver of height h = 70 mm and width a = 140 mm. Impedance analysis at the design frequency of 950 kHz yields an input impedance with a real part of $Re(Z_{11}) \approx 385.5\ \Omega$ and a vanishing reactive part, $Im(Z_{11}) \approx 0$, confirming that the structure is resonant at the intended frequency. Post-processing of the complex port voltages and currents gives a power transfer efficiency (PTE) of 65.8% for the baseline receiver configuration; subsequent optimization of the receiver coil geometry raised this value to 72.87%. Magnetic field maps show a peak field of approximately 2.8 A/m, concentrated around the vertical conductive elements. It is emphasised that the resonant input impedance of ≈385.5 Ω is not matched to the 50 Ω source, so a dedicated matching network — realised through lumped reactive elements integrated into the resonator — is a prerequisite for physical implementation. The study is entirely numerical; the resulting design requirements and the scope of the experimental validation still needed are set out in detail.*

Keywords: *wireless power transfer; volumetric resonator; ubiquitous charging; smart home; power transfer efficiency; impedance matching; lumped elements; CST Studio Suite.*

1. Introduction

Wireless power transfer (WPT) has developed from short-range inductive coupling between closely spaced coils into a family of techniques aimed at powering devices throughout an entire living space [1], [3], [6]. Commercial inductive charging remains dominated by planar pad architectures, in which the receiver must be placed directly on, or immediately above, the transmitter coil. Three limitations follow from this

geometry. Lateral or angular misalignment causes a rapid fall in efficiency; the magnetic field is reasonably uniform only within a thin layer close to the pad surface, so that pronounced hot spots and dead zones appear when the field is examined across a three-dimensional volume; and the usable transfer range is confined to a few millimetres to centimetres, which precludes simultaneous charging of several devices distributed across a room.

The concept of ubiquitous charging addresses these constraints by converting an entire volume — a drawer, a tabletop, or a room — into an active charging zone, within which multiple receivers can be powered irrespective of their precise position and orientation [3], [8], [10]. Quasistatic cavity resonators, Helmholtz-type coil arrangements, metasolenoids, and split-loop structures have all been proposed as candidate architectures, each offering a distinct compromise between field uniformity, working volume, quality factor, fabrication complexity, and human-exposure safety [2]–[5], [9], [11].

The present work contributes to this line of research a room-scale volumetric resonator dimensioned for a standard domestic room and intended as the basis for a physical smart-home charging prototype. The objectives are: (i) to establish, through full-wave simulation, that the proposed structure is resonant at the target operating frequency; (ii) to quantify the power transfer efficiency achievable with a compact receiver and the effect of receiver geometry on that efficiency; (iii) to characterise the spatial distribution of the magnetic field within the working volume; and (iv) to define, on the basis of the simulated port impedance, the lumped-element matching and tuning requirements that must be satisfied before a physical prototype can be built. Because the study rests entirely on numerical simulation, its results are presented as design-stage predictions rather than as validated performance figures; the limitations of this position are discussed in Section 5.

2. Materials and Methods

2.1 System configuration

The resonator was dimensioned to occupy a standard domestic room, 3.35 × 3.35 × 2.5 m, so that the simulated scenario corresponds directly to a realistic ubiquitous-charging environment rather than to a scaled laboratory fixture. The resonant structure comprises vertical conductive elements distributed at the periphery of the volume, interconnected so as to sustain a circulating magnetic field within the enclosed space. The design operating frequency was set to 950 kHz, a value chosen to fall within the range in which conductor losses remain moderate while the wavelength remains much larger than the structure, keeping the system firmly in the quasistatic regime.

The receiver was modelled as a compact coil of height h = 70 mm and width a = 140 mm, representative of a unit that could be embedded in a consumer device or a small appliance, and terminated in a port for the extraction of complex voltage and current.

2.2 Numerical model

Electromagnetic analysis was performed in CST Studio Suite. The structure was excited at a transmitter port and the response sampled at a receiver port, giving a two-port network from which impedance and scattering parameters were extracted. Field monitors were placed within the volume to record the magnetic and electric field distributions at the operating frequency.

It should be stated explicitly that the impedance and efficiency results reported in Section 3 were evaluated at the single design frequency of 950 kHz rather than over a swept band. This is sufficient to characterise performance at the nominal operating point, but it does not by itself establish the width of the resonance or the quality factor of the structure; the implications are addressed in Section 5.

2.3 Efficiency evaluation

Power transfer efficiency was obtained by post-processing the complex voltage and current at each port, as the ratio of the real (active) power delivered to the receiver port to the real power accepted at the transmitter port. This definition accounts for the phase relationship between voltage and current and therefore excludes circulating reactive power, which in a high-Q resonant structure may substantially exceed the transferred active power.

3. Results

3.1 Input impedance and resonance

Figure 1 shows the simulated input impedance at the transmitter port. At 950 kHz the real part attains $\mathrm{Re}(Z_{11}) \approx 385.5\ \Omega$ while the imaginary part is effectively zero, $\mathrm{Im}(Z_{11}) \approx 0$. The vanishing reactance confirms that the structure is resonant at the intended design frequency, the inductive and capacitive contributions of the resonator cancelling at this point.

This result must, however, be interpreted carefully. Resonance and impedance matching are distinct conditions. A purely real input impedance of approximately 385.5 Ω indicates resonance, but it is substantially higher than the 50 Ω reference impedance of a standard source. In the absence of a matching network, the corresponding reflection coefficient magnitude is $|\Gamma| = |385.5 - 50| / |385.5 + 50| \approx 0.77$, so roughly 59% of the incident power would be reflected at the port rather than delivered into the resonant volume. The design therefore requires an impedance transformation stage, the realisation of which is treated in Section 4.

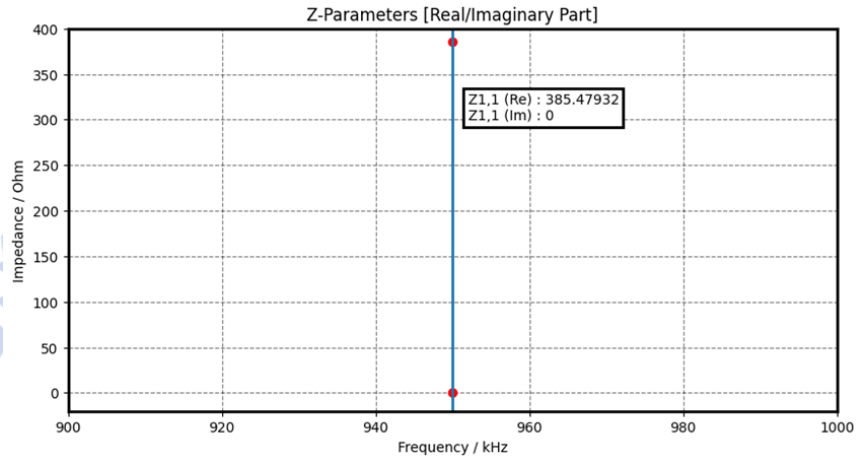


Figure 1. Simulated input impedance Z_{11} at the transmitter port, evaluated at 950 kHz. The real part reaches ≈385.5 Ω and the imaginary part vanishes, confirming resonance at the design frequency.

3.2 Power transfer efficiency

Figure 2 shows the power transfer efficiency computed from the complex port quantities. For the baseline receiver configuration the efficiency at 950 kHz is 0.658, that is 65.8%. Subsequent optimization of the receiver coil geometry, carried out by iteratively varying the receiver radius while holding the transmitter structure and operating frequency fixed, raised the efficiency to 72.87% — an improvement of approximately seven percentage points obtained without any modification to the transmitting infrastructure. This is a practically significant result, since in a deployed system the transmitter is fixed once installed whereas receivers embedded in different devices may be re-dimensioned freely.

For completeness, a preliminary configuration evaluated at 1.2 MHz during an earlier stage of the work exhibited a return loss of $S_{11} = -12.44$ dB. This value pertains to that earlier configuration and should not be attributed to the 950 kHz design reported here, for which the return loss before matching follows directly from the impedance mismatch quantified in Section 3.1.

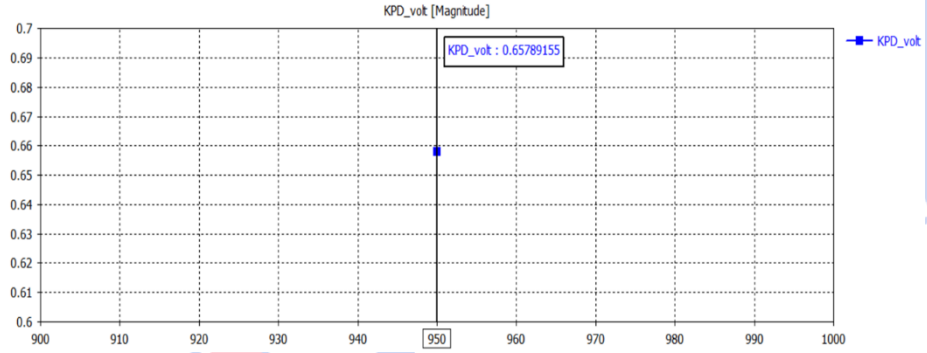


Figure 2. Power transfer efficiency evaluated from the complex port voltages and currents at 950 kHz, giving PTE = 0.658 (65.8%) for the baseline receiver configuration.

3.3 Magnetic field distribution

Figure 3 presents the magnetic field distribution in a horizontal cross-section of the working volume, together with the corresponding colour scale. The field reaches a maximum of approximately 2.8 A/m. The distribution is markedly non-uniform: the field is strongly concentrated around the four vertical conductive elements at the periphery of the structure, while the central region of the cross-section exhibits a considerably weaker field. The receiver, visible near the centre of the section, is therefore located in a comparatively low-field region in this particular configuration.

Two consequences follow. First, since the achievable efficiency depends on the local field strength at the receiver, placing the receiver nearer to the high-field regions would be expected to increase coupling, at the cost of increased position sensitivity — which runs counter to the objective of position-independent charging. Second, the non-uniformity evident in Figure 3 means that a single peak field value is an incomplete descriptor of the working volume; a quantitative uniformity metric evaluated over a defined charging zone is required, and is identified in Section 5 as necessary further work.

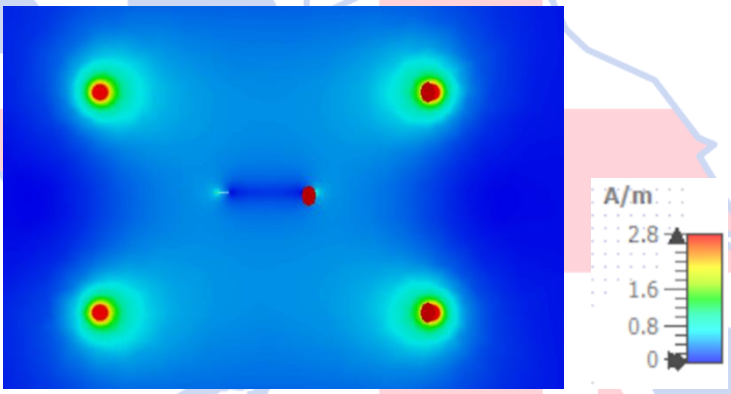


Figure 3. Magnetic field distribution in a horizontal cross-section of the resonator volume at 950 kHz (left), with the corresponding colour scale in A/m (right). The field peaks at approximately 2.8 A/m around the vertical conductive elements.

4. Lumped-Element Matching and Tuning

The impedance result of Section 3.1 defines the principal requirement for physical realisation: the resonant input impedance of approximately 385.5 Ω must be transformed to the 50 Ω source impedance if the reflected power is to be reduced to an acceptable level. This is to be accomplished through discrete reactive components integrated into the resonator structure, an approach standard in resonant WPT systems [4], [7].

Three implementation steps are foreseen. The first is port matching, in which series and parallel reactive elements are introduced at the receiver and transmitter ports to perform the required impedance transformation; candidate component values

have been identified in the simulation model, and their final selection will be fixed against the measured impedance of the fabricated structure. The second is the creation of physical gaps in the conductive elements, realised in the model by Boolean subtraction and physically by interrupting the conductor to provide soldering points for the components. The third is tuning, that is, compensation of the parasitic capacitance and inductance introduced by the physical assembly — supports, joints, fasteners, and the surrounding environment — so that the resonance remains centred at 950 kHz after construction.

It should be noted that the component values extracted from the simulation model are model-specific and will require adjustment against measurement, since the parasitic contributions of a physical build are not fully represented in the numerical model. In particular, the voltage rating of the capacitors must be selected with regard to the high reactive voltages that develop across the gaps of a high-Q resonant structure, which may considerably exceed the nominal supply voltage.

5. Discussion and Limitations

The results establish that the proposed room-scale structure is resonant at the intended frequency and that a compact receiver placed within the volume can achieve an efficiency of 65.8%, rising to 72.87% after receiver-geometry optimization. Considering that the receiver is small relative to the enclosed volume and is not constrained to a fixed alignment with a transmitting pad, these figures compare favourably with the efficiencies typically reported for mid-range and volumetric WPT architectures [3], [7], [10], and support the viability of the volumetric approach for smart-home charging.

Several limitations must nevertheless be stated plainly, as they bound the conclusions that may legitimately be drawn.

- The study is entirely numerical. No physical prototype has been fabricated or measured. All values reported here are simulation outputs obtained in a single software environment, subject to the idealisations of the model — nominal material properties, idealised boundary conditions, and a simplified receiver load.
- The reported impedance and efficiency were evaluated at a single frequency rather than across a swept band. The resonance bandwidth and the loaded quality factor of the structure therefore remain undetermined, although both are decisive for the sensitivity of the system to component tolerance and environmental detuning. A frequency sweep across a band encompassing the resonance is the most immediate extension of this work.
- The structure is resonant but not matched. The efficiency figures reported in Section 3.2 characterise transfer between the ports of the simulated network;

the end-to-end efficiency of a physical system will additionally depend on the performance of the matching network and of the power-conversion stages, and will be lower.

- Field uniformity has not been quantified. Figure 3 shows a visibly non-uniform distribution, and the claim of position-independent charging cannot be substantiated without a uniformity metric evaluated over a defined working volume — for instance the coefficient of variation of the field magnitude sampled across a regular grid.
- Human exposure has not been assessed in the present work. Since the intended application places the resonator in an occupied domestic room, a dosimetric evaluation against the exposure limits of IEEE Std C95.1-2019 [12] using anatomically realistic phantoms is a mandatory prerequisite to any physical deployment, not an optional refinement.

Taken together, these points position the present study as a design-stage feasibility analysis. It establishes the operating point, quantifies the efficiency attainable in simulation, and defines the matching requirement that governs physical realisation, while leaving bandwidth characterisation, uniformity quantification, safety assessment, and experimental validation to subsequent work.

6. Conclusion

A room-sized volumetric resonator occupying a 3.35 × 3.35 × 2.5 m space and operating at 950 kHz has been designed and analysed by full-wave simulation. The structure is resonant at the design frequency, exhibiting a purely real input impedance of approximately 385.5 Ω. A compact receiver of dimensions h = 70 mm and a = 140 mm achieves a power transfer efficiency of 65.8%, increasing to 72.87% after optimization of the receiver geometry alone. The magnetic field within the volume peaks at approximately 2.8 A/m and is concentrated around the vertical conductive elements. The principal design requirement identified for physical realisation is an impedance transformation from the resonant 385.5 Ω to the 50 Ω source, to be implemented through lumped reactive elements integrated into the structure together with tuning to compensate for the parasitics of the physical assembly. Future work will address the characterisation of the resonance bandwidth and quality factor through a frequency sweep, the quantification of field uniformity across a defined charging volume, dosimetric safety assessment against IEEE Std C95.1-2019, and the construction and measurement of a physical prototype.

References

1. Kurs A. et al. Wireless power transfer via strongly coupled magnetic resonances // Science. 2007. Vol. 317, No. 5834. P. 83–86.
2. Chakram S. et al. Seamless high-Q microwave cavities for multimode quantum systems // Physical Review Letters. 2021. Vol. 127, No. 10. P. 107701.
3. Chabalko M. J., Sample A. P. Quasistatic cavity resonance for ubiquitous wireless power transfer // PLOS ONE. 2017. Vol. 12, No. 2. e0170535.
4. Sample A. P., Meyer D. T., Smith J. R. Analysis, design, and implementation of an adaptive wireless power transfer system // IEEE Transactions on Industrial Electronics. 2013. Vol. 60, No. 2. P. 570–581.
5. Lipworth G. et al. Magnetic metamaterial superlens for increased range wireless power transfer // Scientific Reports. 2014. Vol. 4. P. 5491.
6. Song M., Belov P., Kapitanova P. Wireless power transfer based on dielectric resonators with high permittivity // Applied Physics Letters. 2016. Vol. 109, No. 22. P. 223902.
7. Hui S. Y. R., Zhong W., Lee C. K. A critical review of recent progress in mid-range wireless power transfer // IEEE Transactions on Power Electronics. 2014. Vol. 29, No. 9. P. 4500–4511.
8. Zhang J., Zhao J., Zhang Y. Ubiquitous wireless power transfer: a review of multi-degree-of-freedom systems // IEEE Transactions on Power Electronics. 2021. Vol. 36, No. 3. P. 2510–2525.
9. Smirnov P. et al. Wireless power transfer based on the magnetic field enhancement in a dielectric resonator // IEEE Antennas and Wireless Propagation Letters. 2021. Vol. 21, No. 1. P. 193–197.
10. Massignani A. et al. 3-D wireless power transfer for smart environments using room-sized resonators // IEEE Transactions on Industrial Electronics. 2021. Vol. 68, No. 11. P. 10772–10781.
11. Rancani A. et al. Optimization of field uniformity in quasistatic cavity resonators for WPT // IEEE Antennas and Wireless Propagation Letters. 2023. Vol. 22, No. 4. P. 844–848.
12. IEEE Standard for Safety Levels with Respect to Human Exposure to Radio Frequency Electromagnetic Fields, 0 Hz to 300 GHz. IEEE Std C95.1-2019. 2019. P. 1–312.